Forcing mechanism of the Pleistocene east Asian monsoon variations in a phase perspective

TIAN Jun[1,2], WANG Pinxian[1], CHENG Xinrong[1], WANG Rujian[1] & SUN Xiangjun[1,3]

1. State Key Laboratory of Marine Geology, Tongji University, Shanghai 200092, China;
2. Institute of Geology and Geophysics, Chinese Academy of Sciences, Beijing 100029, China;
3. Institute of Botany, Chinese Academy of Sciences, Beijing 100093, China
Correspondence should be addressed to Tian Jun (email: ian.tianjun@263.net)

Received January 13, 2004; revised June 28, 2004

Abstract The deep sea records from the ODP Sites 1143 and 1144 in the northern and southern South China Sea (SCS), including foraminiferal δ^{18}O and δ^{13}C, Opal% and pollen percentage, reveal that the variations of the east Asian monsoon have been closely correlated with the variations of the Earth's orbital parameters (eccentricity, obliquity and precession) and the global ice volume on orbital scale. All the monsoonal proxies show strong 100 ka, 41 ka and 23 ka cycles. Although *G. ruber* δ^{13}C of Site 1143 is coherent with the ETP (ETP= normalized (eccentricity + obliquity-precession) at eccentricity, obliquity and precession bands, most of the coherent relationship focuses on the precession band, and the other monsoonal proxies are coherent with the ETP only at the precession band, which indicate that precession dominates the Pleistocene tropical climate changes. The phase relationship of the monsoonal proxies with the foraminiferal δ^{18}O implies that the global ice volume changes have played a significant role in modulating the east Asian monsoon climate, at least dominating the winter monsoon. This forcing mechanism of the east Asian monsoon is apparently different from that of the Indian ocean monsoon. The variations of the east Asian monsoon at the precession band, at least that of the winter monsoon, have been controlled not only by the sensible heating but also by the latent heating of the surface water in the South China Sea.

Keywords: South China Sea, ODP, east Asian monsoon, orbital forcing, global ice volume.

DOI: 10.1360/01yd0467

The variations of the Earth's geometry (ETP) predominate climate changes such as monsoon on the Earth[1], serving as its external forcing. The loess/paleosol sequence in Central China provides a good record of terrestrial deposition to study the evolution of the east Asian monsoon[2−4]. However, the deep sea deposition, due to its high resolution dating and abundant climate proxies, should be able to provide more climatic information in the geological time, such as the forcing mechanism of the east Asian monsoon, which describes the relationship of the east Asian monsoon with the orbital forcing and the global ice volume changes. The east Asian monsoon and the Indian Ocean monsoon comprise the two important components of the Asian monsoon system. By the study of the Arabian Sea deposition, Clemens et al.[5] found that the Earth's geometry (ETP) serves as the external forcing of the Indian Ocean summer monsoon whereas the latent heat across the equator from the southern Indian Ocean to the northern serves as the internal

forcing; in addition, he also found that the global ice volume changes have little impact on the evolution of the Indian Ocean summer monsoon, conflicting with the previous GCM simulation results[6,7]. Previous works by Wang et al.[8] presume that the east Asian monsoon bears a similar forcing mechanism to that of the Indian Ocean summer monsoon. Being restricted to the past four glacial/interglacial cycles, the work by Wang et al.[8] cannot reveal the truth in the whole Pleistocene. Is the forcing mechanism of the east Asian monsoon really similar to that of the Indian Ocean summer monsoon? To get satisfied answers, we need to obtain high resolution and longer deep sea records in the SCS. In this paper, we will present some climate records from ODP Site 1143 in the southern SCS and Site 1144 in the northern SCS, and further study their coherent and phase relationship with the orbital forcing and the global ice volume changes on three orbital cycles (100 ka, 41 ka and 23 ka).

1 Materials and methods

The deep sea sediments from ODP Site 1143 were sampled at intervals of 10 cm, with a time resolution of 2 ka. We measured planktonic foraminiferal *G. ruber* δ^{18}O and δ^{13}C[9] as well as Opal percentage[10] in each sample, of which all the records span the past 1.6 Ma. The age model of Site 1143 is based on the astronomical tuning of the benthic δ^{18}O[11]. For ODP Site 1144, the records spanning the past 1 Ma include *G. ruber* δ^{18}O[12] and the pollen records[13] (*Pinus*% and Herbs%), with a time resolution varying from 154 a to 1160 a, on average 820 a.

The cross spectral analyses will be used to explore the coherent and phase relationship on orbital periods among different time series. Coherency and phase are two important parameters for cross spectral analysis. Coherency is a measure of the linear correlation between two time series over a given frequency when the phase difference is set to zero. Statistically significant coherence over a given frequency band indicates a strong linear relationship between two variables. Phase estimates over a specific frequency band indicate temporal (lead/lag) relationships between variables. Coherence estimates, in conjunction with the phase relationships, could allow one to draw inferences about physical relationships between potential forcing mechanisms and climate response[5]. "ARAND" package is used to do the cross spectral analyses.

2 The Earth's geometry (ETP), global ice volume and east Asian monsoon proxies

The astronomical solution of Berger and Loutre[14] is used to obtain the changes of the Earth's geometry in the geological time. The foraminiferal shell's δ^{18}O records the waxing and waning of the Northern Hemisphere Ice Sheet in the Pleistocene[5], thus it can be used as the proxy of the global ice volume changes. The east Asian monsoon proxies are from Sites 1143 and 1144.

2.1 ODP Site 1143 in the southern SCS

The opal flux (including radiolarian and diatom) usually implies the modern ocean productivity[15]. The monsoon-driven upwelling can improve the siliceous productivity of the upper ocean. In the Indian Ocean, the opal flux denotes the changes of the intensity of the Indian Ocean summer monsoon[5]. Whereas in the SCS, the siliceous productivity indicated by Opal% is also connected to the east Asian monsoon changes[16,17]. The sediment trap studies in the northern and central SCS show that the Opal flux shows peak values in both winter and summer monsoon seasons[18]. Thus, the Opal% of Site 1143 can be used as the proxy of the east Asian monsoon. At Site 1143, the Opal% is lower before 400 ka, ranging from 1.5% to 2.5%, with smaller glacial/interglacial amplitude; after 400 ka, the Opal% increases abruptly, ranging from 1.5% to 6.0%, with larger glacial/interglacial amplitude (Fig. 1). In general, the Opal% of Site 1143 is lower during glacials but higher during interglacials.

When the nutrient-rich subsurface water upwells to the surface by the monsoon, the δ^{13}C of the sea surface water will decrease. If the foraminiferal shell equilibrates with the ambient water during the process of its calcification, the changes of the shell's δ^{13}C should record the changes of the monsoon intensity. In the SCS, in the areas off the northwest coast of the Philippines and off the south coast of the Vietnam,

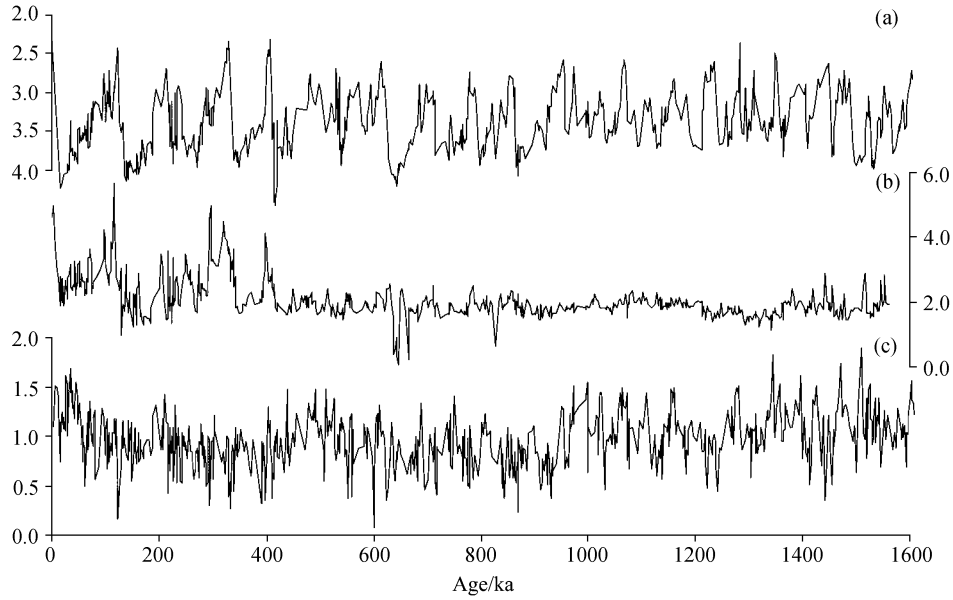

Fig. 1. Paleo-climate records of ODP Site 1143 in the southern South China Sea. (a) Benthic foraminiferal *Cibicidoides* δ^{18}O (‰, PDB)[11]; (b) Opal percentage (%)[10]; (c) 1.6 Ma Planktonic foraminiferal *G. ruber* δ^{13}C (‰, PDB).

which are affected by winter monsoon induced upwelling and summer-monsoon induced upwelling respectively, the δ^{13}C of core-top *G. ruber* and *P. obliquiloculata* show relatively lower values than in other areas[8]. The planktonic foraminifer *G. ruber* δ^{13}C for the past 1.6 Ma varies from 0.2‰ to 2.0‰ (Fig. 1). The glacial/interglacial change of *G. ruber* δ^{13}C is not so obvious as that of the benthic δ^{18}O. The high-frequency and large amplitude fluctuations of the *G. ruber* δ^{13}C of Site 1143 may be related to the summer and winter monsoon variations.

2.2 ODP Site 1144 in the northern SCS

The vegetation in southeast China and Taiwan Island are two important sources of the pollen deposition in the northern SCS[13]. The modern pollen distribution in surface sediments of the northern SCS is marked by very high percentages (<90% of the total pollen sum) and concentrations of tree pollen, in which *Pinus* is absolutely dominant[19]. The maximal values of concentration of tree pollen occur in the northwest adjacent to the convergence of the Bashi and Taiwan Straits, rather than near estuaries of big rivers, and stretch as a saddle from NE to SW in completely concordant with the direction of the NE winter monsoon and surface current. Such a distribution pattern implies that tree pollen, especially pine, adapted to wind transport and water flotation, are mainly brought by the NE winter monsoon and wind-driven currents from large source areas, probably including south and southeast China (Sun et al., 2003). During glacials when the continent was drier and herbs were more flourishing, herbs replacing pine become the dominant pollen grains to be transported by the winter monsoon. Therefore, the Herbs and *Pinus* found in the deep sea sediments of Site 1144 were probably transported by the strong winter monsoon driven circulation[13], and thus can be used as the proxies of the east Asian winter monsoon. The *Pinus* and Herb pollen of Site 1144 has a reverse relationship. The sum of their abundance exceeds 50%, comprising the principal part of the pollen assemblage. In general, the *Pinus*% is higher during interglacials but lower during glacials, whereas the Herbs% is higher during glacials but lower during interglacials (Fig. 2). The time resolution of the pollen records is about 150 a after 400 ka but 1100 a before 400 ka.

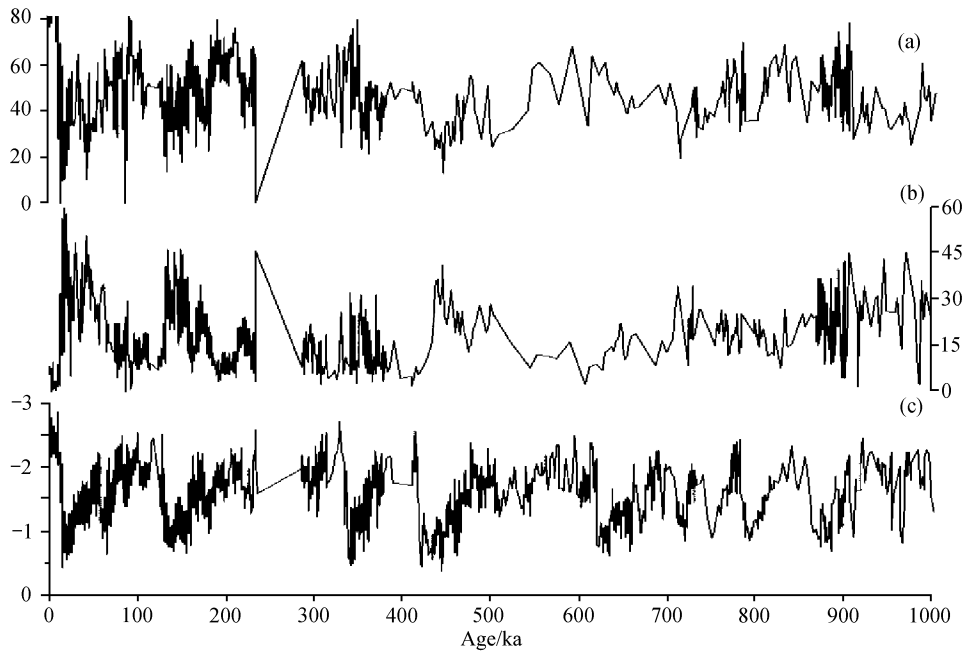

Fig. 2. Paleo-climate records of ODP Site 1144 in the northern South China Sea. (a) *Pinus* percentage (%)[13]; (b) Herbs percentage (%)[13]; (c) Planktonic foraminiferal *G. ruber* δ^{18}O (‰, PDB)[12]. The age model is based on the *G. ruber* δ^{18}O of ODP Site 1144[12].

3 Cross spectral analyses of the climate proxies

3.1 Coherencies of Herbs% and *Pinus*% from Site 1144 with the ETP and δ^{18}O

The cross spectral analyses indicate that, although the pollen records in the past 1 Ma (Herbs% and *Pinus*%) demonstrate strong variances at the 100 ka band and moderate to strong variances at the 41 ka and 23 ka bands, they are coherent with the Earth's geometry (ETP) only at the 23 ka precession band (Fig. 3(a), (b); Table 1). The upper ocean temperature contrast of the southern SCS is coherent with the ETP only at the precession band[1)], so does that of the east tropical Pacific[20]. These indicate that the tropical climate, such as the variations of the thermocline and east Asian winter monsoon in the SCS, is externally controlled by the precession radiation.

The Herbs% and *Pinus*% are highly coherent with the global ice volume change (represented by foraminiferal-δ^{18}O) at the 100 ka and the 23 ka bands (Fig. 3(c), (d); Table 1). Though the cross spectrum between the pollen records and the δ^{18}O shows no coherent relationship at the 41 ka band, a highlighted coherency stands at the 54 ka band, a heterodyne frequency of the primary orbital periods. A similar coherent relationship at the 54 ka band also exists between the Indian Ocean monsoon tracers and the concentration of the orbital variance[5]. The 100 ka glacial cycles are dominant in the Earth's Pleistocene climate records[21], especially in the foraminiferal δ^{18}O records. Both the Herbs% and the *Pinus*% of Site 1144 display perfect glacial-interglacial variations for the past 1 Ma. The graphic structure of the pollen records, which is identical to that of the δ^{18}O, in conjunction with the cross spectral analyses, indicates that the east Asian winter monsoon has been greatly influenced by and coherent with the global ice volume change. The inference is consistent with the conclusions drawn from the loess-paleosol sequence[22,23] and the north Pacific dust concentration[24] as well as from numeri-

1) Tian Jun, Plio-Pleistocene climate variations in foraminiferal stable isotope records at ODP Site 1143, South China Sea, Ph.D Thesis of Tongji University, 2003.

Table 1 Coherency and phase relationship of the east Asian monsoon proxies of ODP Site 1143 with the orbital forcing (ETP) and the global ice volume variations (foraminiferal-δ^{18}O) in the Pleistocene[a)]

	100 ka (eccentricity)		41 ka (obliquity)		23 ka (precession)	
	coherency	phase	coherency	phase	coherency	phase
ETP vs – δ^{18}O	0.85	23°±17°	0.98	60°±5.6°	0.96	78°±7.8°
ETP vs – Herbs%	—	—	—	—	0.81	176°±20°
ETP vs *Pinus*%	—	—	—	—	0.77	150°±22°
ETP vs Opal%	—	—	—	—	0.80	162°±20.3°
ETP vs δ^{13}C	0.93	–41.5°±12°	0.82	107°±19.3°	0.95	147°±9.4°
–δ^{18}O vs – Herbs%	0.8	–10°±20°	—	—	0.79	46°±21°
–δ^{18}O vs *Pinus*%	0.85	9°±16°	—	—	0.85	27°±17°
–δ^{18}O vs Opal%	0.92	–32°±11.5°	0.82	8°±19.3°	0.83	78°±18.8°
–δ^{18}O vs δ^{13}C	—	–63°±38°	0.88	52°±14.9°	0.9	78°±14.1°

a) 80% coherency = 0.707267. "—" denotes the coherencies less than 0.707267.

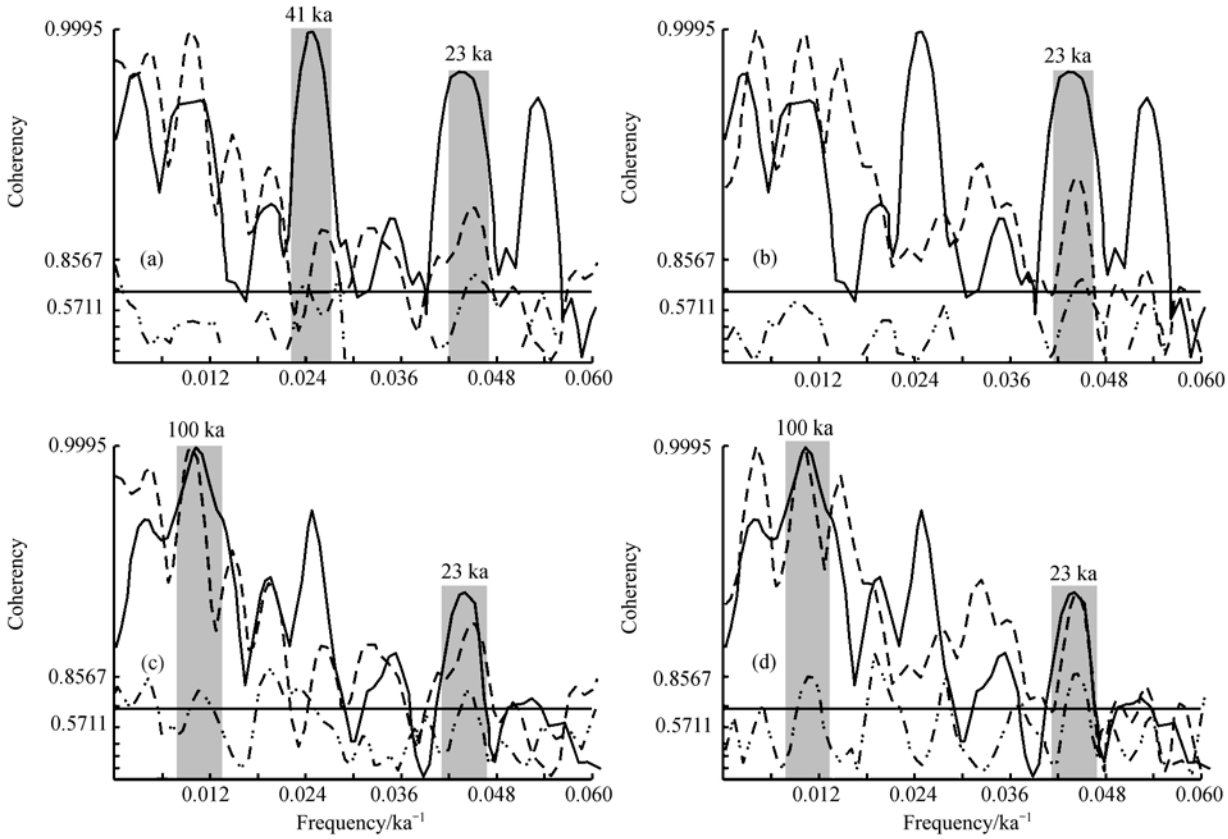

Fig. 3. Cross spectral analyses of the pollen records of ODP Site 1144 with the orbital forcing (ETP) and the global ice volume variations (δ^{18}O) (0—1 Ma). (a) ETP vs Herbs%; (b) ETP vs *Pinus*%; (c) δ^{18}O vs Herbs%; (d) δ^{18}O vs *Pinus*%. Solid lines denote the spectrums of ETP or δ^{18}O. Dashed lines denote the spectrums of the pollen records. Dotted dashed line denotes coherency. The spectral density is plotted on log scale. The coherency is plotted on hyperbolic arctangent scale. The horizontal solid lines denote the coherencies above 80% standard level. The grey bars denote the orbital period of 100 ka, 41 ka and 23 ka.

cal simulations[6]. As the other important component of the Asian monsoon system, the Indian Ocean summer monsoon appears to be different, with proxies not coherent with the global ice volume change at the 100 ka band but at the 41 ka and the 23 ka bands. In addition, the fact that the ice-volume minima (maximum effectiveness of sensible heating) lags behind the Indian Ocean summer monsoon maxima by 33 ka over

the eccentricity band, excludes a forcing-response relationship between the Northern Hemisphere Glaciation and the Indian Ocean summer monsoon changes[5].

3.2 Coherencies of Opal% and *G. ruber* δ^{13}C from Site 1143 with the ETP and δ^{18}O

Both *G. ruber* δ^{13}C and Opal% of Site 1143 are coherent with the concentration of orbital variance at the three primary orbital cycles, the 100 ka, the 41 ka and the 23 ka bands (Fig. 4(a), (b); Table 1). Particularly, the coherency of *G. ruber* δ^{13}C with the ETP at the 23 ka precession band is the highest, nearly two times the coherency at the eccentricity or obliquity band. Also, the coherency of Opal% with the ETP at the 23 ka precession band is the highest among the three coherencies. These mean that the strongest responses of the east Asian monsoon to the orbital forcing occur at the precession band. This kind of relationship between the east Asian monsoon proxies and the orbital forcing highlights the precession as the primary force driving the tropical climate change.

The Opal% of Site 1143 is also highly coherent with the $-\delta^{18}$O at the three primary orbital cycles; in addition, the *G. ruber* δ^{13}C is also strongly coherent with the $-\delta^{18}$O at the 41 ka band and the two precession bands (23 ka and 19 ka). Though the coherency of *G. ruber* δ^{13}C with the $-\delta^{18}$O at the 100 ka band does not exceed the 80% statistical level, a strong 100 ka cycle also occurs in its spectrum. The coherent

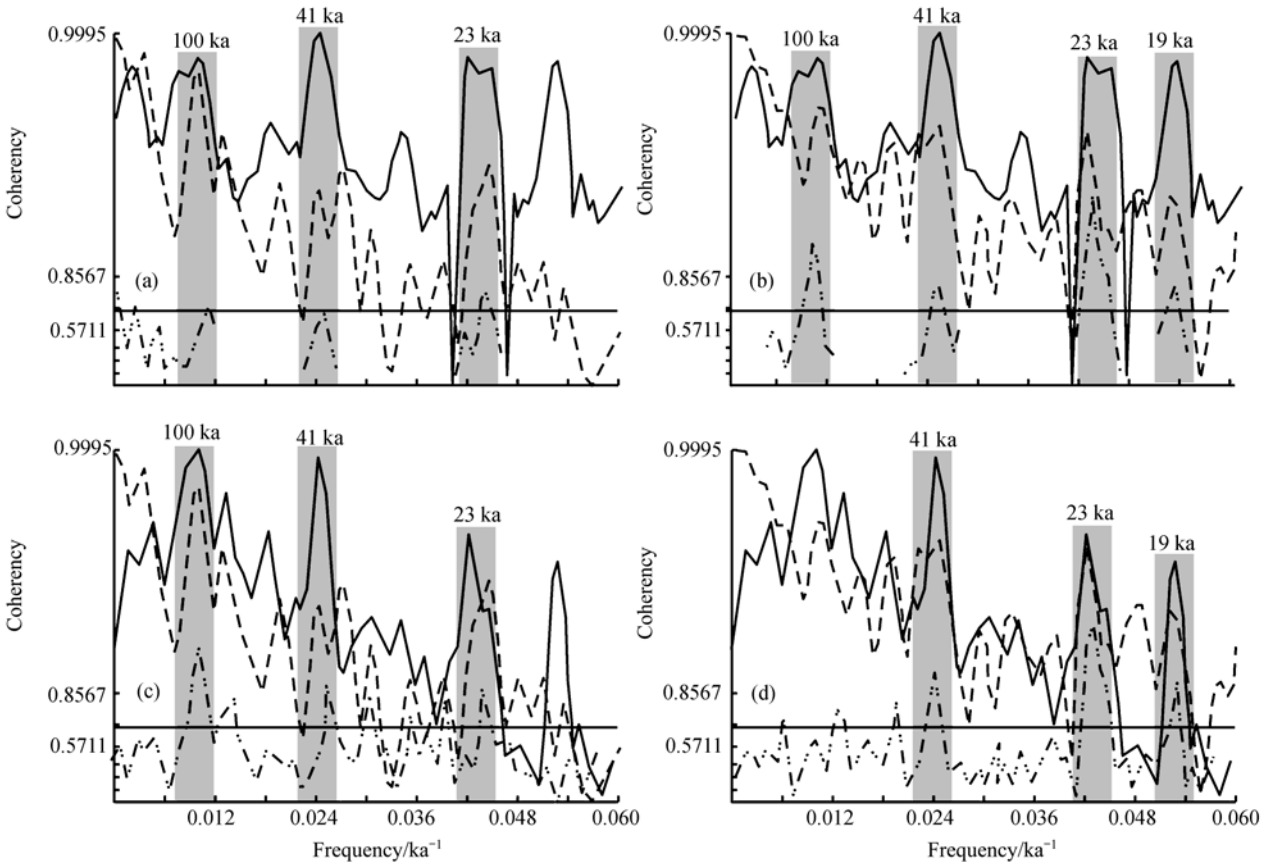

Fig. 4. Cross spectral analyses of *G. ruber* δ^{13}C and Opal% of ODP Site 1143 with the orbital forcing (ETP) and the global ice volume variations (δ^{18}O) (0—1.6 Ma). (a) ETP vs Opal%; (b) ETP vs δ^{13}C; (c) δ^{18}O vs Opal%; (d) δ^{18}O vs δ^{13}C. Solid lines denote the spectrums of ETP or δ^{18}O. Dashed lines denote the spectrums of the pollen records. Dotted dashed line denotes coherency. The spectral density is plotted on log scale. The coherency is plotted on hyperbolic arctangent scale. The horizontal solid lines denote the coherencies above 80% standard level. The grey bars denote the orbital period of 100 ka, 41 ka and 23 ka.

relationship of the Opal% and *G. ruber* δ^{13}C with the $-\delta^{18}$O is consistent with that between the pollen records and the $-\delta^{18}$O, revealing a close relationship between the east Asian monsoon variations and the global ice volume change.

3.3 Phase

The phase wheels in Fig. 5 demonstrate the phase relationships of the proxies with the ETP at the primary orbital cycles. At the 100 ka band, as seen from Fig. 5(a) and Table 1, the global ice volume minima as represented by $-\delta^{18}$O lags behind the Northern Hemisphere insolation maximum by $23° \pm 17°$, roughly equal to 6.4 ± 4.7 ka; the Opal% leads the ETP by $2.9° \pm 24°$, close to zero; and the *G. ruber* δ^{13}C leads the ETP by $41.5° \pm 12°$, roughly equal to 11.5 ± 3.2 ka. The nearly zero-phase between Opal% and ETP indicates an in-phase relationship of the east Asian monsoon with the orbital forcing, whereas the relatively big phase between *G. ruber* δ^{13}C and ETP at this band rules out this in-phase relationship. As introduced above, the pollen record is not coherent with the ETP at the 100 ka band. The non-coherent relationships, together with the phase relations, rule out a linear response of the east Asian monsoon to the orbital forcing at the eccentricity band. The phase wheels as shown in Fig. 6(a) demonstrate that the phases of −Herbs% and *Pinus*% with $-\delta^{18}$O at the 100 ka band are −10° and 9° respectively, which can be taken as zero phase if taking into account of the phase errors. This indicates that the global ice volume change is just in phase with the east Asian winter monsoon change at the eccentricity band. Although a coherent relationship exists between the Opal% and $-\delta^{18}$O also at this band, the negative phase as big as 32° indicates a lead of the Opal% relative to the global ice volume change at the eccentricity band. The phases of the pollen records with the $-\delta^{18}$O at least demonstrate that the east Asian winter monsoon is greatly influenced by the global ice volume change.

At the 41 ka band, all monsoon tracers and the global ice volume change are coherent with the concentration of the orbital variance (ETP) (Fig. 5(b)). Their phases relative to the ETP are close to each other if considering the phase errors. This means that the orbital forcing has almost the same controls over the east Asia monsoon and the global ice volume change at the 41 ka band. If taking the average phase of the monsoon proxies as the best estimate of the east Asia monsoon response to the orbital forcing, the average of the four monsoon tracers indicates that the maxima of the monsoon strength occur ~10000 a after the

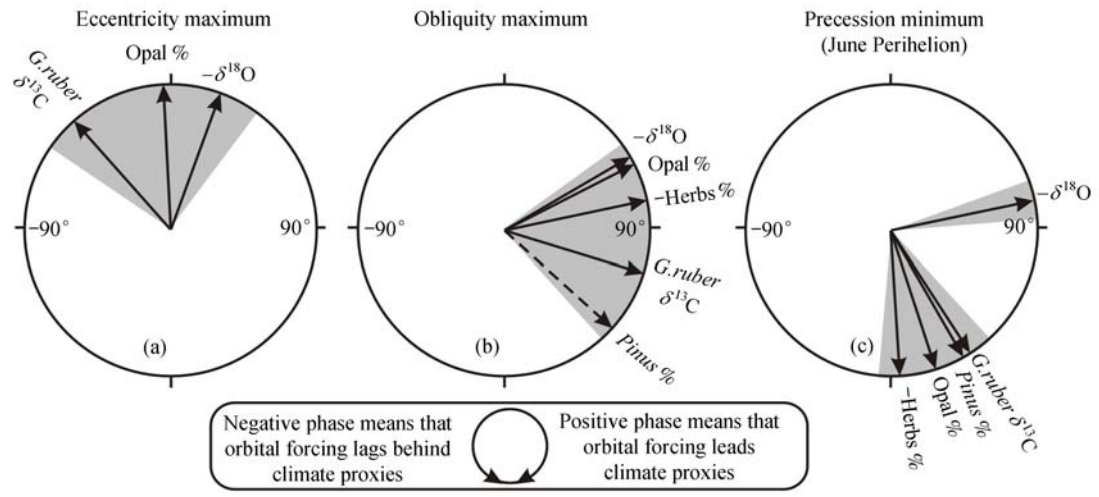

Fig. 5. Phase relationship of the east Asian monsoon proxies from ODP Site 1143 and 1144 with the orbital forcing (ETP) at the three orbital periods in the Pleistocene. (a) 100 ka; (b) 41 ka; (c) 23 ka. Solid arrows denote the coherency above 80% statistical level. Dashed arrows denote the coherency lower than 80% statistical level.

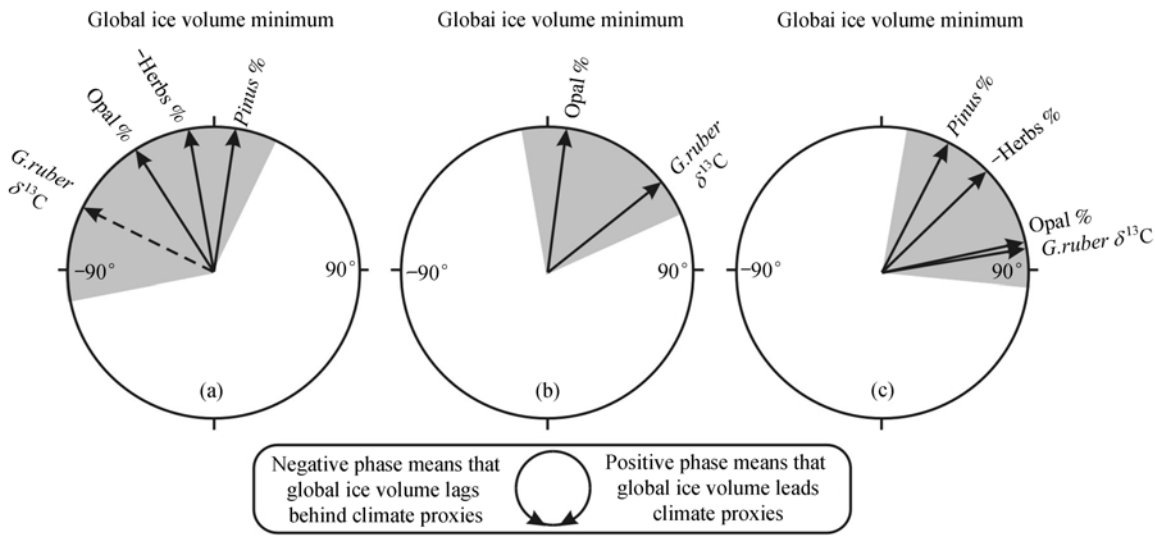

Fig. 6. Phase relationship of the east Asian monsoon proxies from ODP Site 1143 and 1144 with the global ice volume variations (foraminiferal δ^{18}O) at the three orbital periods in the Pleistocene. (a) 100 ka; (b) 41 ka; (c) 23 ka. Solid arrows denote the coherency above 80% statistical level. Dashed arrows denote the coherency lower than 80% statistical level.

maxima of the obliquity radiation (10000 a lag = (94°/360°)×41000 a), and occur ~3872 a after the minimum of the global ice volume change at the 41 ka band (3872 a = ((94°– 60°)/360°)×41000 a). If the radiation or the global ice volume change was the sole forcing, one would expect a near zero phase lag. The lag indicates that, in addition to the radiation forcing and the Northern Hemisphere Glaciation forcing, some other forcing mechanisms internal to the monsoon system should be also responsible for the east Asia monsoon changes. Fig. 6(b) demonstrates the phase relationships between the monsoon variations and the global ice volume change over the 41 ka band. Both of the Opal% maxima and the *G. ruber* δ^{13}C maxima lag behind the global ice volume minima at the 41 ka band, by about 910 a and 5900 a respectively. However, the pollen records are not coherent with the $-\delta^{18}$O at this band.

As shown in Fig. 5(c) and Table 1, the phases of the four monsoon proxies relative to ETP are much closer at the precession band than at the obliquity band, but they departure away from the phase of the $-\delta^{18}$O relative to the ETP. The average of the phases of Herbs% and *Pinus*% relative to the ETP indicates that the maxima in the east Asian winter monsoon occurs about 10 ka after the maxima of the precession radiation. The average of the phases of the four monsoon tracers relative to the ETP indicates that the maxima in the east Asian monsoon occurs about 10 ka after the maxima of the precession radiation. Taking the average of the – Herbs% and *Pinus*%, at the precession band, the east Asian winter monsoon strength maxima occurs about 2332 a after the global ice volume minima (Fig. 6(c); Table 1). It is at the precession band that all monsoon tracers recorded at Site 1143 and 1144 demonstrate similar coherency and phase relationships with the orbital forcing and the global ice volume change. In the Arabian Sea, the maxima of the Indian Ocean summer monsoon strength occurs ~8000 a after the maxima of the precession radiation[5], and occurs ~2500 a after the minima of the global ice volume, but occurs simultaneously with minimum cold-season SSTs in the southern subtropical Indian Ocean. Therefore Clemens et al.[5] concluded that the 8000-a phase lag between radiation maxima and monsoon maxima can be accounted for, in part, by increased effectiveness of sensible heating, but, as a whole, by increased latent heat heating. From the coherency and phase analysis, the east Asian monsoon,

at least the winter monsoon, is also affected, in part, by the increased effectiveness of sensible heating, but as a whole, is affected by another mechanism? The 10 ka phase lag of the east Asian monsoon relative to the radiation forcing at the precession band may be accounted for as a whole, by the increased latent heat or combined influences of multiple factors. Further work needs to be done.

4 Conclusion

The four time series of the east Asian monsoon proxies demonstrate three major orbital cycles in the Pleistocene, but they are coherent with the concentration of the orbital variance (ETP) only at the precession band. Although *G. ruber* δ^{13}C is coherent with the ETP at the three orbital cycles, most of the coherent relationship occurs at the precession band. These indicate that the tropical climate, such as the variations of the thermocline and east Asian monsoon in the SCS, is externally controlled by the precession radiation. The coherency and phase relationship of the monsoon proxies indicate that the east Asian monsoon, at leas the winter monsoon, is greatly influenced by the global ice volume change. It is at the precession band that all monsoon tracers recorded at Site 1143 and 1144 demonstrate similar coherency and phase relationships with the radiation forcing and the global ice volume change. The east Asian monsoon, at least the winter monsoon, is affected, in part, by the increased effectiveness of sensible heating, but as a whole, is affected by another mechanism? This mechanism may be the increased latent heat or combined influences of multiple factors. The previous conclusion by Wang et al.[8] that the east Asian monsoon bears a similar forcing mechanism to that of the Indian Ocean monsoon, should be revised. At least on orbital scale, the relationship of the east Asian monsoon with the global ice volume changes is different from that of the Indian Ocean monsoon.

Acknowledgements These samples were provided by the Ocean Drilling Program (ODP). ODP is sponsored by the U.S. National Science Foundation (NSF) and participating countries under management of Joint Oceanographic Institutions (JOI), Inc. This research was supported by the National Natural Science Foundation of China (Grant Nos. 40476027, 40306011, 4999560 and 40321603) and the National Key Basic Research Special Foundation (Grant No. G2000078500).

References

1. Hays, J. D., Imbrie, J., Shackleton, N. J., Variations in the earth's orbit: pacemaker of the ice ages, Science, 1976, 194: 1121－1132.
2. Liu, T., Loess and Environment, Beijing: Ocean Press, 1985, 1－215.
3. Kukla, G., Loess stratigraphy in central China, Quaternary Science Reviews, 1987, 6: 191－219.[DOI]
4. Kukla, G., Heller, F., Liu, X. M. et al., Pleistocene climates in China dated by magnetic susceptibility, Geology, 1988, 16: 811－814. [DOI]
5. Clemens, S. C., Prell, W., Murray, D. et al., Forcing mechanisms of the Indian Ocean monsoon, Nature, 1991, 353: 720－725. [DOI]
6. Kutzbach, J. E., Guetter, P. J., The influence of changing orbital parameters and surface boundary conditions on climate simulations for the past 18000 years, J. Atmos. Sci., 1986, 43: 1726－1759. [DOI]
7. Prell, W. L., Kutzbach, J. E., Monsoon variability over the past 150000 years, J. Geophys. Res., 1987, 92: 8411－8425.
8. Wang, L., Sarnthein, M., Erlenkeuser, H. et al., East Asian monsoon climate during the late Pleistocene: high-resolution sediment records from the South China Sea, Marine Geology, 1999, 156: 245－284. [DOI]
9. Wang, P., Tian, J., Cheng, X., Transition of Quaternary glacial cyclicity in deep-sea records at Nansha, the South China Sea, Science in China, Ser. D, 2001, 44(10): 926－933.
10. Wang, R. J., Li, J., Quaternary high-resolution opal record and its paleo-productivity implication at ODP Site 1143, southern South China Sea, Chinese Science Bulletin, 2003, 48(4): 363－367.
11. Tian, J., Wang, P. X., Cheng, X. R. et al., Astronomically tuned Plio-Pleistocene benthic δ^{18}O records from South China Sea and Atlantic-Pacific comparison, Earth and Planetary Science Letters, 2002, 203: 1015－1029. [DOI]
12. Bühring, C., Sarnthein, M., Erlenkeuser, H., Toward a high-resolution stable isotope stratigraphy of the last 1.1 million years: Site 1144, South China Sea, Proc. ODP. Sci. Results, 2003, 184, in press.
13. Sun, X. J., Luo, Y. L., Huang, F. et al., Deep-sea pollen from the South China Sea: Pleistocene indicators of East Asian monsoon, Marine Geology, 2003, 201: 97－118. [DOI]
14. Berger, A., Loutre, M. F., Insolation values for the climate of the last 10 million years, Quaternary Science Review, 1991, 10: 297－317. [DOI]
15. Dickens, G., Barron, J., A rapid deposited pinnate diatom ooze in Upper Miocene-Lower Pliocene sediment beneath the North Pacific polar front, Marine Micropaleontology, 1997, 31: 177－182. [DOI]
16. Wang, R. J., Clemens, S., Huang, B. Q. et al., Quaternary palaeoceanographic changes in the northern South China Sea (ODP Site 1146): radiolarian evidence, Journal of Quaternary Science, 2003, 18(8): 745－756. [DOI]
17. Wang, R. J., Abelmann, A., Radiolarian responses to paleoceanographic events of the southern South China Sea during the Pleis-

tocene, Marine Micropaleontology, 2002, 46: 25－44. [DOI]
18. Tian, J., Wang, P. X., Cheng, X. R., Development of the East Asian monsoon and Northern Hemisphere glaciation: Oxygen isotope records from the South China Sea, Quaternary Science Reviews, 2004, in press.
19. Sun, X., Li, X., Beug, H. J., Pollen distribution in hemipelagic surface sediments of the South China Sea and its relation to modern vegetation distribution, Marine Geology, 1999, 156: 211－226. [DOI]
20. Ravelo, A., Shackleton, N. J., Evidence for surface-water circulation changes at site 851 in the eastern tropical Pacific Ocean, Proc. ODP Sci. Results, 1995, 138: 503－514.
21. Imbrie, J., Boyle, E., Clemens, S. et al., On the structure and origin of major glaciation cycles, 1, Linear responses to Milankovitch forcing, Paleoceanography, 1992, 7: 701－738.
22. Sun, D. H., An, Z. S., Shaw, J. et al., Magnetostratigraphy and palaeoclimatic significance of Late Tertiary aeolian sequences in the Chinese Loess Plateau, Geophys. J. Int., 1998, 134: 207－212. [DOI]
23. An, Z. S., Kutzbach, J. E., Prell, W. L. et al., Evolution of Asian Monsoons and Phased uplift of the Himalaya-Tibetan Plateau since Late Miocene Times, Nature, 2001, 411: 62－66. [DOI]
24. Rea, D. K., Snoeck, H., Joseph, L. H., Late Cenozoic eolian deposition in the North Pacifc: Asian drying, Tibetan uplift, and cooling of the Northern Hemisphere, Paleoceanography, 1998, 13: 215－224. [DOI]